Available online at www.sciencedirect.com
ScienceDirect
Journal of Solid State Chemistry 180 (2007) 772–779
JOURNAL OF SOLID STATE CHEMISTRY
www.elsevier.com/locate/jssc

Synthesis, structure, and physicochemical investigations of the new α $Cu_{0.50}TiO(PO_4)$ oxyphosphate

S. Benmokhtar[a], H. Belmal[a], A. El Jazouli[a,*], J.P. Chaminade[b], P. Gravereau[b], S. Pechev[b], J.C. Grenier[b], G. Villeneuve[c], D. de Waal[d]

[a]*Laboratoire de Chimie des Matériaux Solides (LCMS), Université Hassan II Mohammedia, Faculté des Sciences Ben M'Sik, Casablanca, Morocco*
[b]*Institut de Chimie de la Matière Condensée de Bordeaux (ICMCB-CNRS), Université de Bordeaux1, 33608 Pessac, France*
[c]*CRPAA, UMR 5060, Université Bordeaux, 33607-CNRS Pessac, France*
[d]*Department of Chemistry, University of Pretoria, 0002 Pretoria, South Africa*

Received 13 July 2006; received in revised form 10 October 2006; accepted 25 October 2006
Available online 17 November 2006

Abstract

The room-temperature crystal structure of a new Cu(II) oxyphosphate—α $Cu^{II}_{0.50}TiO(PO_4)$—was determined from X-ray single crystals diffraction data, in the monoclinic system, space group $P2_1/c$. The refinement from 5561 independent reflections lead to the following parameters: $a = 7.5612(4)$Å, $b = 7.0919(4)$Å, $c = 7.4874(4)$Å, $\beta = 122.25(1)^\circ$, $Z = 4$, with the final $R = 0.0198$, $wR = 0.0510$. The structure of α $Cu^{II}_{0.50}TiO(PO_4)$ can be described as a $TiOPO_4$ framework constituted by chains of tilted corner-sharing $[TiO_6]$ octahedra running parallel to the *c*-axis and cross linked by phosphate $[PO_4]$ tetrahedra, where one-half of octahedral cavities created are occupied by Cu atoms. Ti atoms are displaced from the center of octahedra units in alternating long (2.308 Å) and short (1.722 Å) Ti–O(1) bonds along chains. Such O(1) atoms not linked to *P* atoms justify the oxyphosphate formulation α $Cu_{0.50}TiO(PO_4)$. The divalent cations Cu^{2+} occupy a Jahn–Teller distorted octahedron sharing two faces with two $[TiO_6]$ octahedra. EPR and optical measurements are in good agreement with structural data. The X-ray diffraction results are supported by Raman and infrared spectroscopy studies that confirmed the existence of the infinite chains –Ti–O–Ti–O–Ti–. α $Cu_{0.50}TiO(PO_4)$ shows a Curie–Weiss paramagnetic behavior in the temperature range 4–80 K.

Keywords: Crystal structure; Oxyphosphate; Copper compound; Magnetism; EPR; Vibrational spectra; Jahn–Teller effect

1. Introduction

Inorganic phosphate materials represent a wide field of investigation which appears promising for various applications. Potassium titanyl phosphate $KTiO(PO_4)$ (KTP) [1] and many of its structural materials, have important applications in non-linear optics and electrooptics due to its high non-linear optical and electrooptical coefficients, high optical damage threshold, low dielectric constants and chemical stability [2–4]. Its structure consists of 3D network of PO_4 tetrahedra and TiO_6 octahedra linked by corners. The TiO_6 octahedra are linked by corners and form chains (helices) along [0 1 1] and [0 $\bar{1}$ 1] directions, with alternating short and long Ti–O bonds. These chains are tilted and present cis and trans Ti–O connections. The off center displacement of Ti atoms gives rise to electric moments. All the TiO_6 chains are parallel and it induces a non-centrosymmetrical space group ($Pna2_1$) and consequently non-linear optical and ferroelectric properties.

In recent study, a new family of titano-oxyphosphates of formulation $M^{II}_{0.5}TiO(PO_4)$ and $Li_{1-2x}M_x{}^{II}TiO(PO_4)$ was synthesized for M^{II} = Ni, Co, Fe … [5–8]. In order to complete the study of this family it appeared interesting to investigate the copper member $Cu^{II}_{0.50}TiO(PO_4)$.

Below we present the results of the synthesis, single crystal structure and physicochemical investigation of the new low temperature form of the oxyphosphate $Cu^{II}_{0.50}TiO(PO_4)$ named α, by means of X-ray diffraction, EPR,

*Corresponding author. Fax: +212 22704675.
E-mail addresses: a.eljazouli@univh2m.ac.ma, eljazouli_abdelaziz@yahoo.fr (A. El Jazouli).

0022-4596/$ - see front matter © 2006 Published by Elsevier Inc.
doi:10.1016/j.jssc.2006.10.040

diffuse reflection, magnetic measurements, Raman and infrared spectroscopy. The structural determination of α $Cu^{II}_{0.50}TiO(PO_4)$ on single crystal is the first study on a compound of the $M^{II}_{0.50}TiO(PO_4)$ series; it confirms the ab initio study done on the powder of $Ni_{0.50}TiO(PO_4)$ [6].

2. Experimental

Divalent copper–titanium oxyphosphate α $Cu_{0.50}TiO(PO_4)$ was prepared by coprecipitation using the same method that was previously applied to the synthesis of $Co_{0.5}Ti_2(PO_4)_3$ [9]. To obtain ≈1 g of α $Cu_{0.50}TiO(PO_4)$, stoichiometric quantities of $Cu(NO_3)_2.3H_2O$ (I) and $NH_4H_2PO_4$ (II) were dissolved separately in distilled water ($V \approx 20$ ml). $TiCl_4$ was diluted in ethanol, in air. The concentration of this alcoholic solution (III) was 41.1 mg/l. A slow addition under stirring of (III) in (I + II) mixture, at room temperature, induces a precipitation. The blue gel recovered was maintained at 70 °C until the solution had completely been evaporated, then progressively heated to 400 °C and kept at this temperature for 18 h. The blue product obtained was found amorphous until 600 °C. Its crystallization began around 700 °C. The final treatment was done at 950 °C, in oxygen atmosphere, during 18 h.

Single crystals were prepared by heating the powder near the temperature of decomposition (~1000 °C) in a platinum crucible, then followed by slow cooling to 500 °C at rate of 3 °C/h and finally cooled to room temperature by turning off the furnace power, clear light blue crystals corresponding to the formula α $Cu_{0.50}TiO(PO_4)$ were obtained.

The new phase, α $Cu_{0.50}TiO(PO_4)$, was also obtained as microcrystalline powder by solid-state reaction employing CuO, TiO_2 and $NH_4H_2PO_4$. Stoichiometric amounts of these reagents, ground in agate mortar, were heated in a first step at 250 °C in a porcelain crucible to decompose $NH_4H_2PO_4$ and remove the volatile species. Then, successive treatments at 400, 600, 800 and 950 °C, for 24 h each, were performed. The blue-crystallized powder at the end of the process was a single phase as shown by the good agreement of the X-ray powder pattern (Table 1) of the bulk product with that calculated from single crystal data.

X-ray powder diffraction (XRPD) spectra were recorded at room temperature by using a X'PERT MPD (PANALYTICAL) diffractometer (Cu$K\alpha$ radiation, $\lambda =$ 1.54184 Å; 40 kV and 40 mA). Single crystal X-ray diffraction data were obtained on a BRUKER-KAPPA-CCD diffractometer with graphite monochromator (Mo$K\alpha$ radiation, $\lambda = 0.71073$ Å; 30 kV and 50 mA).

The possibility of phase transition with temperature was investigated by X-ray diffraction (HTXRD) with ANTON-PAAR HTK16 furnace mounted on a X'PERT MPD (PANALYTICAL) diffractometer, and a heating rate of 20 °C/h.

Density of α $Cu_{0.50}TiO(PO_4)$ was experimentally determined using bromobenzene as immersion liquid. The obtained value ($d_{meas.} = 3.71$ g/cm^3) agrees with the calculated one ($d_{calc.} = 3.73$ g/cm^3).

Table 1
X-Ray powder diffraction data of α $Cu_{0.50}TiO(PO_4)$ ($\lambda K\alpha_1$ (Cu) = 1.5406 Å)

h	k	l	$d_{obs.}$	$d_{calc.}$	$100I/I_0$
1	0	0	6.393	6.395	30
1	1	0	4.746	4.749	23
0	2	0	3.545	3.546	7
2	1	−1	3.334	3.335	27
1	1	−2	3.307	3.308	100
1	1	1	3.233	3.234	49
2	0	0	3.198	3.197	36
0	2	−1	3.093	3.094	40
2	1	−2	2.988	2.987	10
0	1	2	2.893	2.891	5
2	2	−1	2.585	2.586	23
1	2	−2	2.574	2.573	20
3	3	−2	2.486	2.487	14
2	2	−2	2.413	2.413	7
2	2	0	2.377	2.375	8
2	1	−3	2.331	2.331	11
3	1	−1	2.319	2.319	17
2	1	1	2.262	2.262	10
1	3	0	2.213	2.217	12
0	3	1	2.216	2.215	12
3	1	−3	2.098	2.098	5
3	1	0	2.042	2.041	6
1	2	−3	2.001	2.002	5
1	3	1	1.982	1.981	4
4	0	−2	1.900	1.889	6
4	1	−2	1.825	1.825	5
3	0	−4	1.817	1.817	3
2	1	−4	1.808	1.808	4
1	0	−4	1.773	1.773	2
4	1	−3	1.769	1.769	3
3	3	−1	1.703	1.703	4
2	2	−4	1.654	1.654	12
4	2	−3	1.623	1.624	9
3	2	−4	1.617	1.617	8
3	3	−3	1.607	1.608	7
2	4	−1	1.605	1.605	5
4	0	0	1.599	1.599	6
0	0	4	1.582	1.583	12

EPR spectra were recorded using a Bruker Spectrometer operating in the X-band frequency ($\nu \approx 9.5$ GHz). The magnetic field was scanned between 250 and 360 mT. DPPH ($g = 2.0036$) and MgO were used as field markers.

The diffuse reflectance spectra were recorded at 300 K between 210 and 2400 nm using a double monochromator Cary 2400 spectrometer.

The magnetic measurements were performed using a SQUID magnetometer (Quantum Design MPMS2). The magnetizable was measured as a function of temperature ($4.2 \leq T \leq 300$ K) and of magnetic field ($0 \leq H \leq 3$ T).

The Raman spectrum was recorded under the microscope of a Dilor XY Multichannel spectrometer. Excitation was accomplished with the 514.5 nm line of an argon-ion laser. Incident power was approximately 100 mW at the source, and 10% of that at the sample.

The infrared spectra were recorded using a Bruker IFS 113 v FT-IR spectrometer. Samples were in the form of KBr (mid-IR) and polyethylene (far-IR) pellets.

3. Resolution of the structure

3.1. Single-crystal X-ray diffraction

A light blue crystal ($60 \times 80 \times 110\,\mu m$) was selected for the structure determination. The cell parameters reported in Table 2 were determined from a KAPPA-CCD collect with a least squares refinement based upon 2883 reflections with $5.8^\circ < 2\theta < 70^\circ$. The systematic absences $l = 2n+1$ for $(h0l)$ and $k = 2n+1$ for $(0k0)$ are consistent only with space group $P2_1/c$ ($N^\circ 14$). The intensity of each reflection was corrected for background and for Lorentz and polarization effects. Empirical absorption corrections were applied using SCALEPACK program [10]. The first 30 frames of data were recollected at the end of the data collection to monitor crystal decay. Scattering factors for neutral atoms and anomalous dispersion corrections for Ti, Cu and P were taken from the International Tables for Crystallography [11]. The structure was solved by direct methods with SHELXS-97 [12] in the monoclinic space group $P2_1/c$. Full-matrix least-squares refinement with anisotropic thermal parameters for all the atoms was carried out with SHELXL-97 [12]. A summary of the crystal data for α $Cu_{0.50}TiO(PO_4)$ is given in Table 2. Final atomic coordinates and anisotropic displacement parameters are listed in Tables 3 and 4, respectively. Selected bond distances and bond angles are given in Table 5.

Table 2
Crystal data and structure refinement for α $Cu_{0.50}TiO(PO_4)$

	Crystal data
Formula	α $Cu_{0.50}TiO(PO_4)$
Formula weight (g/mol)	190.63
Crystal size (μm)	$60 \times 80 \times 110$
Colour	Light blue
Crystal system	Monoclinic
Space group	$P2_1/c$
Temperature	293(2) K
a(Å)	7.5612(4)
b(Å)	7.0919(4)
c(Å)	7.4874(4)
β(°)	122.25(1)°
Volume (Å^3)	339.55(6)
Z	4
Measured density (g/cm^3)	3.71 ± 0.02
Calculated density (g/cm^3)	3.729
Intensity measurements	
Wavelength (Å)	0.71073
Diffractometer	BRUKER–KAPPA–CCD
Scan method	CCD Scans
Absorption coefficient (mm^{-1})	5.92
F(000)	366
θ range (°)	3.5 to 35
Index ranges	$-12 \le h \le 12$, $-11 \le k \le 11$, $-12 \le l \le 12$
Reflections collected [$I > 0\sigma(I)$]	5561
Independent reflections [$I > 0\sigma(I)$]	1474 [R(int) = 0.020]
	1359 reflections with $I > 2\sigma(I)$
Structure solution and refinements	
Absorption correction	Empirical SCALEPACK [9]
Refinement method	Full–matrix least–squares on F^2
Data/parameters refined	1474/71
Goodness of fit on F^2	1.109
Final R indices	$R_1[I > 2\sigma(I)] = 0.0198$, $wR_2[I > 0\sigma(I)] = 0.0510$
Extinction coefficient	0.000(2)
Largest diff. peak and hole (e Å^{-3})	0.53 (near O(4)) and −0.67 (near Cu)

Table 3
Atomic coordinates and equivalent isotropic displacement parameters (Å$^2 \times 10^4$) for α $Cu_{0.50}TiO(PO_4)$

Atom	Wyckoff site	x	y	z	U(eq)
Cu	2a	0	0	0	73(1)
Ti	4e	0.73519(3)	0.21943(3)	0.53513(3)	54(1)
P	4e	0.24896(5)	0.13120(4)	0.74781(5)	50(1)
O(1)	4e	0.7696(2)	0.1511(2)	0.7724(2)	82(2)
O(2)	4e	0.7568(2)	0.0017(2)	0.0935(2)	83(2)
O(3)	4e	0.4410(2)	0.2579(2)	0.8556(2)	93(2)
O(4)	4e	0.2440(2)	0.0189 (2)	0.5709(2)	91(2)
O(5)	4e	0.0544(2)	0.2392(2)	0.1546(2)	75(2)

Table 4
Anisotropic displacement parameters (Å$^2 \times 10^4$) for α $Cu_{0.50}TiO(PO_4)$

Atom	U_{11}	U_{12}	U_{33}	U_{23}	U_{13}	U_{12}
Cu	69(1)	62(1)	70(1)	−7(1)	27(1)	14(1)
Ti	48(1)	59(1)	51(1)	−2(1)	24(1)	1(1)
P	42(2)	51(2)	51(2)	2(1)	22(1)	1(1)
O(1)	97(4)	83(4)	70(4)	9(3)	47(3)	1(3)
O(2)	107(4)	69(4)	87(5)	18(3)	60(4)	9(3)
O(3)	48(4)	94(4)	109(4)	−2(3)	22(3)	−15(3)
O(4)	127(4)	76(5)	87(4)	−14(3)	69(4)	4(3)
O(5)	50(4)	69(4)	94(4)	−19(3)	31(3)	−14(3)

The anisotropic displacement factor exponent takes the form: $-2\pi^2[h^2a^{*2}U_{11} + \cdots + 2hka^*b^*U_{12}]$.

3.2. X-ray powder diffraction

X-ray powder pattern (XRPD) of α $Cu_{0.50}TiO(PO_4)$ was recorded at room temperature in the step scan mode, with the step value of 0.02° and measuring for 30 s at each step. The observed reflections were indexed in a monoclinic unit cell with the following parameters: $a' = 7.5585(3)$ Å, $b' = 7.0888(2)$ Å, $c' = 7.4839(3)$ Å, $\beta' = 122.24(1)^\circ$, in good agreement with the parameters: $a = 7.5612(4)$ Å, $b = 7.0919(4)$ Å, $c = 7.4874(4)$ Å, $\beta = 122.25(1)^\circ$ obtained from the single-crystal X-ray study.

The HTXRD shows a transition from the room temperature α-phase (this study) to a β-phase, reversible

Table 5
Bond distances (Å) and angles (°) for α $Cu_{0.50}TiO(PO_4)$

Ti–O(1)	1.722(1)	O(1)–Ti–O(3)#1	103.3(1)
Ti–O(3)#1	1.895(1)	O(1)–Ti–O(4)#2	100.3(1)
Ti–O(4)#2	1.909(1)	O(1)–Ti–O(2)#3	95.9(1)
Ti–O(2)#3	2.013(1)	O(1)–Ti–O(5)#4	95.3(1)
Ti–O(5)#4	2.099(1)	O(1)–Ti–O(1)#1	165.4(1)
Ti–O(1)#1	2.308(1)	O(3)#1–Ti–O(4)#2	96.1(1)
		O(3)#1–Ti–O(2)#3	90.0(1)
		O(3)#1–Ti–O(5)#4	159.7(1)
		O(3)#1–Ti–O(1)#1	89.2(1)
Cu–O(5)	1.970(1)	O(4)#2–Ti–O(2)#3	160.9(1)
Cu–O(5)#5	1.970(1)	O(4)#2–Ti–O(5)#4	88.3(1)
Cu–O(1)#2	1.979(1)	O(4)#2–Ti–O(1)#1	85.7(1)
Cu–O(1)#6	1.979(1)	O(2)#3–Ti–O(5)#4	80.1(1)
Cu–O(2)#7	2.290(1)	O(2)#3–Ti–O(1)#1	76.2(1)
Cu–O(2)#8	2.290(1)	O(5)#4–Ti–O(1)#1	71.4(1)
O(5)–Cu–O(1)#2	98.5(1)		
O(5)–Cu–O(2)#7	76.5(1)		
O(1)#2–Cu–O(2)#8	77.2(1)		
P–O(3)	1.522(1)		
P–O(4)	1.529(1)		
P–O(2)#2	1.535(1)		
P–O(5)#3	1.549(1)		
O(3)–P–O(4)	110.0(1)		
O(3)–P–O(2)#2	111.4(1)		
O(3)–P–O(5)#3	107.2(1)		
O(4)–P–O(2)#2	110.7(1)		
O(4)–P–O(5)#3	109.9(1)		
O(2)#2–P–O(5)#3	107.5(1)		

Note: Symmetry transformations used to generate equivalent atoms: #1, x, $-y+\frac{1}{2}$, $z-\frac{1}{2}$; #2, $-x+1$, $-y$, $-z+1$; #3, x, $-y+\frac{1}{2}$, $z+\frac{1}{2}$; #4, $x+1$, $-y+\frac{1}{2}$, $z+\frac{1}{2}$; #5, $-x$, $-y$, $-z$; #6, $x-1$, y, $z-1$; #7, $x-1$, y, z; #8, $-x+1$, $-y$, $-z$.

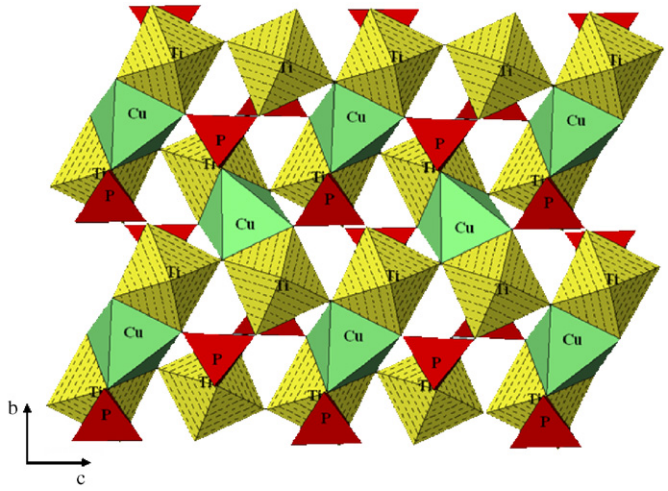

Fig. 1. Projection of the structure of α $Cu_{0.50}TiO(PO_4)$ along the *a*-axis.

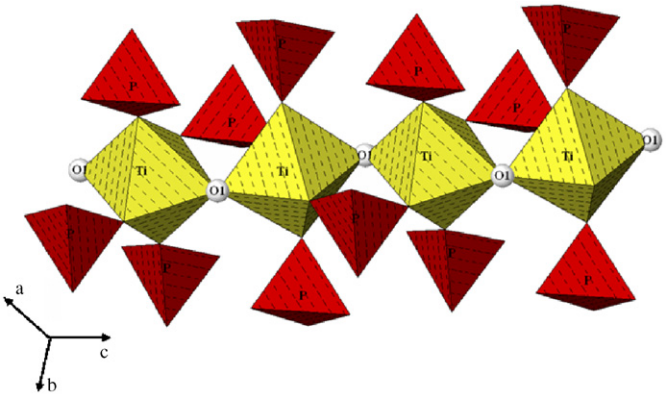

Fig. 2. ($TiOPO_4$) framework in α $Cu_{0.50}TiO(PO_4)$.

but with hysteresis (~600 °C during heating, ~300 °C during cooling).

The β $Cu^{II}_{0.50}TiO(PO_4)$ phase has been obtained stabilized at room temperature in a powder mixture. X-ray diffraction pattern of this powder can be indexed like α-type $P2_1/c$ monoclinic cell: $a = 7.1134(7)$ Å; $b = 7.7282(7)$ Å; $c = 7.3028(7)$ Å; $\beta = 119.30(1)°$. Its crystal structure determination will be reported in the near future.

4. Description of the structure and discussion

The structural framework of α $Cu_{0.50}TiO(PO_4)$ (Fig. 1) appears very similar to that of $Ni_{0.5}TiO(PO_4)$ [6]. It consists of $[TiO_6]_\infty$ octahedral chains running along [001], linked through single $[PO_4]$ tetrahedra. Each $[TiO_6]$ octahedron shares four corners with $[PO_4]$ tetrahedral (Fig. 2). Unlike KTP, the adjacent $[TiO_6]_\infty$ chains in α $Cu^{II}_{0.50}TiO(PO_4)$ are in reverse position (space group $P2_1/c$) and induce compensation of electric moments. This copper oxyphosphate is then antiferroelectric.

The Ti atom is coordinated to six oxygen atoms which form octahedron with bond distances ranging from 1.722 to 2.308 Å. The $[TiO_6]$ octahedra are distorted, linked together by corner to form chains via O(1) atoms so that the sequence of Ti–O(1) bonding in the chains along *c*-axis is alternately long(2.31)–short(1.72)–long(2.31)–short(1.72)···O(1) atoms, not implied in $[PO_4]$ tetrahedra, justify the oxyphosphate designation. The four remaining Ti–O(*i*) ($i = 2, 3, 4, 5$) distances with O(*i*) belonging to the PO_4 groups range between 1.895 and 2.099 Å.

The $[PO_4]$ tetrahedra share oxygen atoms with four $[TiO_6]$ octahedral groups. O(2) and O(4) belong to the same chain while O(3) and O(5) belong to two different chains. Therefore, one $[PO_4]$ group connects three different chains Ti–O–Ti–O–Ti–O. The $[PO_4]$ tetrahedra are isolated each from others and are rather regular with O–P–O bond angle varying from 107.2° to 111.4°. P–O bond distances, ranging between 1.52 and 1.55 Å, are close to those observed for the oxyphosphates $LiTiO(PO_4)$ [13,14] and $Ni_{0.50}TiO(PO_4)$ [6].

The copper atoms are in (2a) crystallographic site. They are surrounded by six oxygen atoms forming an octahedron $[CuO_6]$ located between two faces of two $[TiO_6]$ octahedra of distinct chains. Common triangle faces constituted by O(1), O(2) and O(5) atoms involve longer Ti–O(1) bond (Fig. 3). The $[CuO_6]$ octahedra are distorted

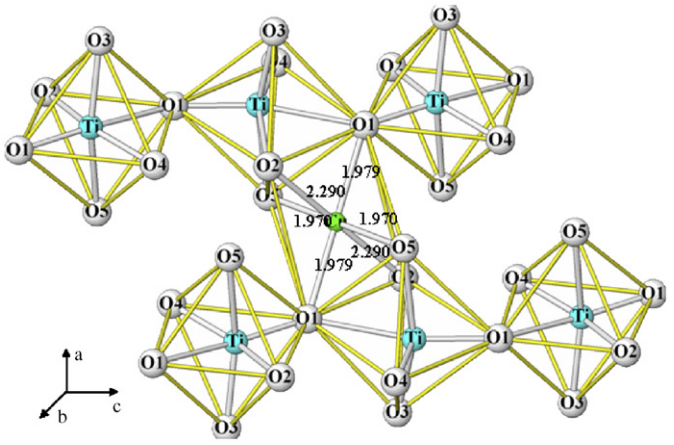

Fig. 3. [CuO_6] octahedron connected to two [TiO_6] chains in α $Cu_{0.50}TiO(PO_4)$.

Table 6
Bond valence calculations for α $Cu^{II}_{0.50}TiO(PO_4)$

	Ti	Cu	P	V_i	V_{theo}
O(1)	1.286	0.444		1.994	2
O(1)	0.264				2
O(2)	0.586	0.192	1.205	2.026	2
O(3)	0.806		1.248	2.099	2
O(4)	0.776		1.225	2.045	2
O(5)	0.464	0.455	1.160	2.121	2
V_i	4.182	2.182	4.838		
V_{theo}	4	2	5	2	

and isolated each from others. The [CuO_6] octahedra exhibit four short equatorial Cu–O bonds in the basal plane (1.970 and 1.979 Å), and two longer apical Cu–O bonds (2.290 Å) (Fig. 3). Moreover, the observed coordination of four short equatorial bonds and two long apical distances is typical of Jahn–Teller distorted coordination configuration ($t^6_{2g}d^2_{z^2}d^1_{x^2-y^2}$) [15]. The Jahn–Teller effect has a strong influence on the resulting parameters cell. The two long Cu–O bonds are almost parallel to (*a*,*c*) plane, so the *a* and *c* parameters are bigger and the *b* parameter lower compared to compounds of the same family $M_{0.50}TiO(PO_4$ (M = Mg, Fe, Co, Ni, Zn). The distance between copper cations ($d^{2+}_{Cu-Cu} = 5.16$ Å) is close to that found for Ni atoms in $Ni_{0.50}TiO(PO_4)$ ($d^{2+}_{Ni-Ni} = 5.18$ Å) [6].

The O(2) and O(5) atoms are bonded to Ti, P, and Cu, whereas O3 and O4 atoms are only bonded to P and Ti. The O(1) atom is connected to two Ti of the same [TiO_6] octahedra chain and to Cu.

To check the validity of the α $Cu_{0.50}TiO(PO_4)$ structure, bond strength sums (denoted V_{sum}) were calculated using the Brown formalism [16,17]. $V_i = \sum_j v_{ij}$ and $v_{ij} = \exp[(R_{ij}-d_{ij})/b]$ with $b = 0.37$ Å, d_{ij}: distance between i and j atoms and R_{ij} is relative to O^{2-}: 1.815 Å for Ti^{4+}, 1.679 Å for Cu^{2+} and 1.604 Å for P^{5+}. The results are in good agreement with the theoretical values for the expected formal oxidation state of Cu^{2+}, Ti^{4+}, P^{5+} and O^{2-} ions (Table 6).

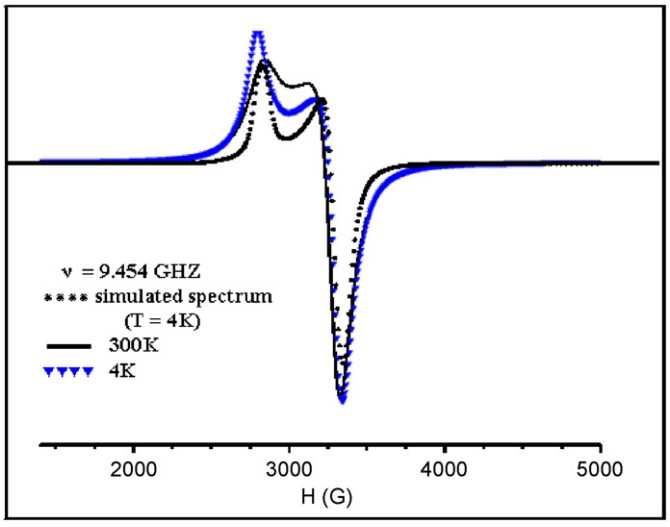

Fig. 4. EPR spectra of α $Cu_{0.5}TiO(PO_4)$ observed at 4 K, 300 K and simulated EPR spectrum at 4 K.

5. Electron paramagnetic resonance investigation (EPR)

The local environment of Cu^{2+} ions in α $Cu^{II}_{0.50}TiO(PO_4)$ was investigated by electron paramagnetic resonance. Fig. 4 shows the X band EPR spectra of α $Cu_{0.5}TiO(PO_4)$ at 4 K and at room-temperature. The EPR spectra are asymmetric, characteristic of Cu^{2+} ions in axially distorted octahedral symmetry (point group D_{4h}). The obtained *g*-values at 4 and 300 K, are respectively: $g_{\|} = 2.37$, $g_{\perp} = 2.06$ ($\bar{g} = 2.168$) and $g_{\|} = 2.367$, $g_{\perp} = 2.096$ ($\bar{g} = 2.184$) $\left(\bar{g} = 1/3\left[\left(g^2_{\|} + g^2_{\perp}\right)^{1/2}\right]\right)$. They are similar to those of $Cu_{0.5}Ti_2(PO_4)_3$ [18], $Cu_{0.5}Zr_2(PO_4)_3$ [19] and $Cu_{0.5}NbAl(PO_4)_3$ [20]. The relationship $g_{\|} > g_{\perp} > 2$ imply that Cu^{2+} ions are coordinated to six ligand atoms in a distorted octahedron, elongated along one axis, which corresponds to the Jahn–Teller distortion ($d^2_{z^2}d^1_{x^2-y^2}$) [15]. These results are in good agreement with structural data which showed that in [CuO_6] octahedron Cu^{2+} ion has two longer Cu–O bonds (~229 Å) and four short Cu–O (~197 Å).

6. Optical absorption studies

Optical absorption spectrum of α $Cu^{II}_{0.50}TiO(PO_4)$, recorded from 200 to 2500 nm at 300 K, is compared to that of TiO_2 rutile (Fig. 5). The spectrum shows two sets of bands, one in small wavelength (UV–Vis) region and another in NIR region. The deconvolution of these bands shows five peaks situated at 282, 411, 791, 977 and 1260 nm (Fig. 5).

The strong absorption band observed in ultraviolet region at 282 nm (35 461 cm^{-1}) is attributed to the $O^{2-} \rightarrow Ti^{4+}$ and $O^{2-} \rightarrow Cu^{2+}$ electronic charge transfers

$$O^{2-}(2p^6) + Ti^{4+}(3d^0) \rightarrow O^{-}(2p^5) + Ti^{3+}(3d^1),$$

$$O^{2-}(2p^6) + Cu^{2+}(3d^1{}_{x2-y2}) \rightarrow O^{-}(2p^5) + Cu^{+}(3d^2{}_{x2-y2}).$$

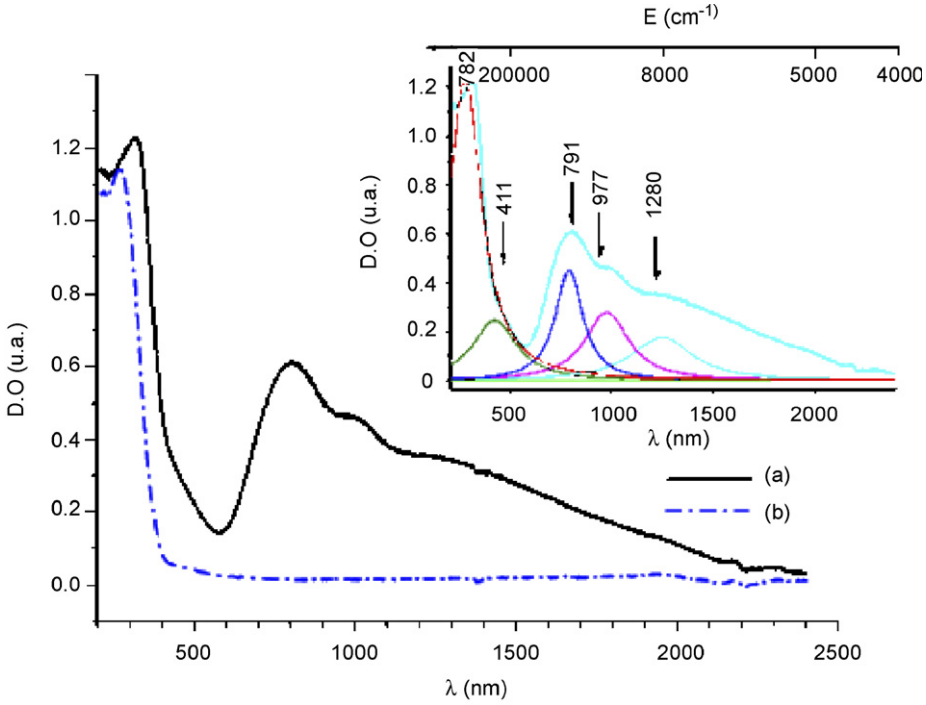

Fig. 5. Absorption spectra of α $Cu_{0.50}TiO(PO_4)$ (a) and TiO_2 (b) at 300 K. The deconvolution of the bands observed in α $Cu_{0.50}TiO(PO_4)$ is shown in the inset.

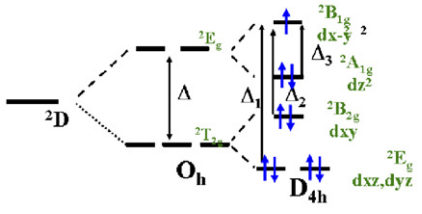

Fig. 6. Energy levels diagram of Cu^{2+} ion (d^9) in D_{4h} symmetry.

The band at 411 nm (24 330 cm^{-1}) is characteristic of Cu(II) in octahedral site and is attributed to the $Cu^{2+} \rightarrow Ti^{4+}$ electronic charge transfer [18]:

$$Cu^{2+}(3d^1{}_{x2-y2}) + Ti^{4+}(3d^0) \rightarrow Cu^{3+}(3d^0{}_{x2-y2}) + Ti^{3+}(3d^1).$$

The bands observed in the visible and infrared regions at 791 nm ($\Delta_1 = 12\,642\ cm^{-1}$), 977 nm ($\Delta_2 = 10\,235\ cm^{-1}$) and 1260 nm ($\Delta_3 = 7936\ cm^{-1}$) correspond to the crystal field transitions between the full occupied states $^2E_g(d_{xz;yz})$, $^2B_{2g}(d_{xy})$ and $^2A_{1g}(d_z^2)$ and the partially occupied level $^2B_{1g}(d_{x^2-y^2})$ of Cu^{2+} ion ($3d^9$) in octahedral site (Fig. 6).

7. Magnetic properties

Fig. 7 shows the thermal variation of the inverse molar magnetic susceptibility χ_m^{-1} of α $Cu^{II}_{0.50}TiO(PO_4)$, between 4.2 and 340 K. At low temperature $\chi_m^{-1} = f(T)$ follows a Curie–Weiss law. Above 100 K the curve becomes progressively concave toward the T-axis. Such a magnetic behavior results from a growing influence of the Van-Vleck temperature-independent paramagnetism term (χ_{vv}) [21], $\chi = C/T - \theta + \chi_{vv}$, which is well fitted with $C = 0.52$, $\theta = 7$ K and $\chi_{vv} = 50 \times 10^{-6}$ uem/mole.

The thermal variation of the Cu^{2+} ion susceptibility in an axial symmetry can be calculated by the usual relationships [22]

$$\chi = \tfrac{1}{3}\chi_{\parallel} + \tfrac{2}{3}\chi_{\perp}$$

with

$$\chi_{\parallel} = \frac{N\beta^2}{3k_BT}\,3\left(1 - \frac{4\lambda_0 k_{\parallel}}{\Delta_1}\right)^2 + \frac{8N\beta^2k_{\parallel}^2}{\Delta_1};$$

$$\chi_{\perp} = \frac{N\beta^2}{3k_BT}\,3\left(1 - \frac{\lambda_0 k_{\perp}}{\Delta_2}\right)^2 + \frac{2N\beta^2k_{\perp}^2}{\Delta_2},$$

where: $\lambda_0 = -830\ cm^{-1}$ is the spin–orbit coupling constant for the free copper ion, $\Delta_1 = 12\,642\ cm^{-1}$ and $\Delta_2 = 10\,235\ cm^{-1}$ are, respectively, the energies of the electronic transitions ^2E_g ($d_{xz;yz}$)$\rightarrow{}^2B_{1g}$ (d_{x2-y2}) and $^2B_{2g}$ (d_{xy})$\rightarrow{}^2B_{1g}$ (d_{x2-y2}), and k the covalence factor. The values of $k_{\parallel}$ and $k_{\perp}$, obtained from the relationships $g_{\parallel} = 2 + 8/\lambda_0/k_{\parallel}^2\big/\Delta_1$ and $g_{\perp} = 2 + 2/\lambda_0/k_{\perp}^2/\Delta_2$, are respectively 0.75 and 0.83. The average susceptibility calculated is: $\chi = 0.47/T + 43 \times 10^{-6} = C/T + \chi_{vv}$. The calculated values of the Curie constant and the Van-Vleck temperature-independent paramagnetism term ($C_{calc.} = 0.47$ and $\chi_{vv\,calc.} = 43 \times 10^{-6}$ uem/mole) are very close to the measured ones ($C_{meas.} = 0.52$ and $\chi_{vv\,meas.} = 50 \times 10^{-6}$ uem/mole). The calculated value of

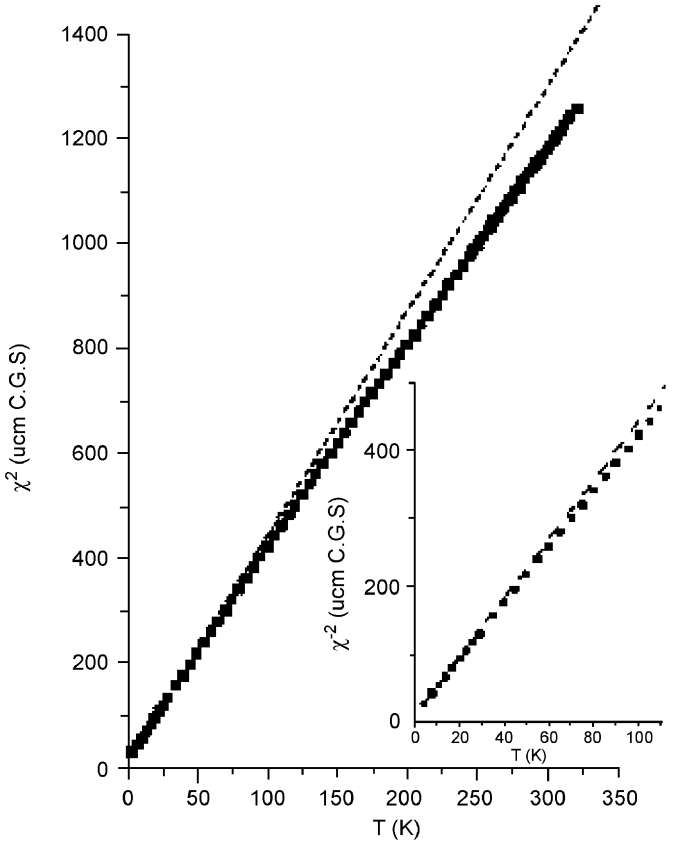

Fig. 7. Thermal variation of the reciprocal paramagnetic susceptibility of α $Cu_{0.50}TiO(PO_4)$.

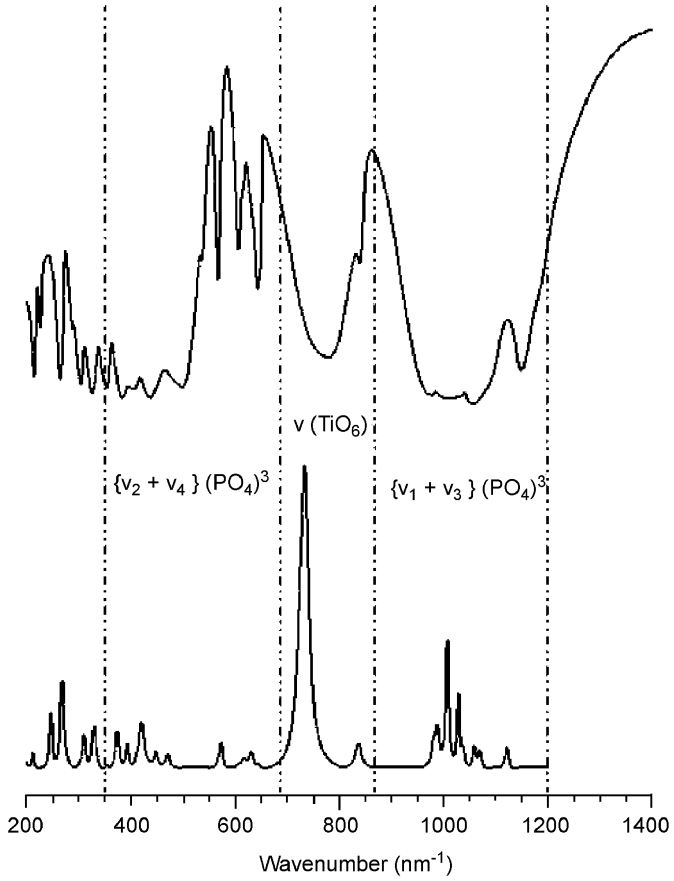

Fig. 8. Raman and infrared spectra of α $Cu_{0.50}TiO(PO_4)$.

the Curie constant $\left(C = Ng^2\beta^2 S(S+1)/3k_B\right)$, using g-values given by EPR spectra, is 0.44.

The low value of the Curie temperature ($\theta p \approx -7$ K) characterizes the existence of weak magnetic interactions between Cu^{2+} ions, which is in good agreement with structural data and the fact that Cu^{2+} ions are located in isolated oxygen distorted octahedra with large Cu–Cu distances ($d^{2+}_{Cu-Cu} = 5.16$ Å).

8. Vibrational spectroscopy

Vibrational analysis for an isolated PO_4^{3-} anion with point group T_d leads to 4 modes: $A_1[(\nu_1$: $\nu_s(PO_4)]$, $E[(\nu_2{:}\delta_s(PO_4)]$ and $2F_2[\nu_3$: $\nu_{as}(PO_4)$ and $\nu_4{:}\delta_{as}(PO_4)]$. All of them are Raman active whereas only ν_3 and ν_4 are infrared active. In α $Cu_{0.50}TiO(PO_4)$ ($P2_1/c$ space group) the phosphor atom is in a C_1 symmetry site; therefore, we expect 8 Raman-active modes for the stretching vibrations, $\nu_1(A_g, B_g) + 3\nu_3$ (A_g, B_g) and 8 IR-active modes, $\nu_1(A_u, B_u) + 3\nu_3(A_u, B_u)$. For the bending vibrations we achieve 10 Raman-active modes, $2\nu_2(A_g, B_g) + 3\nu_4(A_g, B_g)$ and 10 IR-active modes, $2\nu_2(A_u, B_u) + 3\nu_4(A_u, B_u)$. The external modes consist of the translational vibrations of the Ti^{4+}, Cu^{2+} and PO_4^{3-} ions [23–25].

Fig. 8 shows Raman and infrared spectra of α $Cu_{0.50}TiO(PO_4)$. The high wavenumber part (900–1200 cm^{-1}) of the Raman spectrum of α $Cu^{II}_{0.50}TiO(PO_4)$ corresponds to the stretching vibrations of the PO_4 tetrahedra and exhibits 8 peaks (1119, 1069, 1057, 1036, 1026, 1007, 986, 835 cm^{-1}), the predicted ones are eight. In this region of the infrared spectrum, 7 peaks (1146, 1085, 1054, 1025, 1003, 972, 835 cm^{-1}) are observed. For the P–O bending vibrations, seven Raman peaks (571, 470, 445, 417, 392, 371, 353 cm^{-1}) and nine infrared peaks (641, 602, 562, 531, 490, 447, 433, 386, 352 cm^{-1}) are observed, the predicted ones are ten for Raman and infrared. The peaks situated below 300 cm^{-1} are attributed to the external modes.

The strong bands observed in Raman and infrared spectra, respectively, at 732 and 778 cm^{-1} are attributed to the vibrations of Ti–O bonds in the chains [26–28].

9. Conclusion

Crystal structure of α $Cu^{II}_{0.50}TiO(PO_4)$ was determined from single crystal X-ray diffraction data in the monoclinic space group $P2_1/c$. It is constituted by chains of tilted corner-sharing $[TiO_6]$ octahedra running parallel to the c-axis and cross linked by $[PO_4]$ tetrahedra. Cu atoms occupy distorted octahedra ($2a$ sites) located between two $[TiO_6]$ octahedra of two adjacent chains. Ti atoms are displaced

from the center of octahedra units in alternating long (2.308 Å) and short (1.722 Å) Ti–O bonds along chains. Cu^{2+} ion environment with four short equatorial bonds (Cu–O:2×1.970 Å;2×1.979 Å) and two long apical distances (Cu–O:2×2.20 Å) is typical of Jahn–Teller distorted coordination configuration ($t_{2g}^6 d_{z^2}^2 d_{x^2-y^2}^1$). The Jahn–Teller effect has a strong influence on the resulting parameters cell with increase of the *a* and *c* parameters (the two long Cu–O bonds are almost parallel to (*a*, *c*) plan) compared to compounds of the same family $M_{0.50}TiO(PO_4)$ (M = Mg, Fe, Co, Ni, Zn). Powder of α $Cu^{II}_{0.50}TiO(PO_4)$ was characterized by EPR, Raman and infrared spectroscopies and by optical and magnetic measurements. Results are in good agreement with structural data.

Acknowledgements

This work was supported by the "Programme International de Coopération Scientifique, PICS, of CNRST/Morocco–CNRS/France.

References

[1] I. Tordjman, T. Masse, J.C. Guitel, Z. Kristallogr. 139 (1974) 103–115.
[2] Y.S. Liu, D. Dentz, R. Belt, Opt. Lett. 9 (3) (1984) 76–78.
[3] J.D. Bierlein, A. Ferretti, L.H. Brixner, W.Y. Hsu, Appl. Phys. Lett. 50 (18) (1987) 1216–1218.
[4] K.W. Godfrey, P.A. Thomas, B.E. Watts, Mater. Sci. Eng. B 9 (1991) 479–483.
[5] A. El Jazouli, H. Belmal, S. Krimi, B. Manoun, J.P. Chaminade, P. Gravereau, D. de Waal. Proceeding of the 12th International Conference on Solid Compounds of Transition Elements, Saint Malo, 1997.
[6] P. Gravereau, J.P. Chaminade, B. Manoun, S. Krimi, A. El Jazouli, Powder Diffr. 14 (1) (1999) 10–15.
[7] B. Manoun, A. El Jazouli, P. Gravereau, J.P. Chaminade, J.C. Grenier, Ann. Chim. Sci. Mat. 25 (Suppl. i) (2000) S71–S74.
[8] B. Manoun, A. El Jazouli, P. Gravereau, J.P. Chaminade, F. Bourée, Powder Diffr. 17 (4) (2002) 290–294.
[9] R. Olazcuaga, J.M. Dance, G. Le Flem, J. Derouet, L. Beaury, P. Porcher, A. El Bouari, A. El Jazouli, J. Solid State Chem. 143 (1999) 224–229.
[10] Z. Otwinoswski, W. Minor, Macromol. Crystallogr. Part A: Methods Enzymol. 276 (1997) 307–326.
[11] International Tables for Crystallography, vol. IV, Kynoch Press, Birmingham, UK, 1974, p. 72.
[12] G.M. Sheldrick, SHELXS-97, SHELXL-97, University of Göttingen, Germany, 1997.
[13] A. Robertson, J.G. Fletcher, J.M. S Skakle, A.R. West, J. Solid State Chem. 109 (1994) 53–59.
[14] P.G. Nagornoy, A.A. Kapshuck, N.V. Stuss, N.S. Slobodyanik, A.N. Chernega, Z. Neorganicheskoi Khimii 36 (1991) 2766–2768.
[15] H.A. Jahn, E. Teller, Proc. R. Soc. A 161 (1937) 220–235.
[16] I.D. Brown, D. Altermatt, Acta Crystallogr. B 41 (4) (1985) 244–247.
[17] N.E. Brese, M. O'Keeffe, Acta Crystallogr. B 47 (1991) 192–197.
[18] A. El Jazouli, J.L. Soubeyroux, J.M. Dance, G. Le Flem, J. Solid State Chem. 65 (1986) 351–355.
[19] A. El Jazouli, M. Alami, R. Brochu, J.M. Dance, G. Le Flem, P. Hagenmuller, J. Solid State Chem. 71 (1987) 444–450.
[20] M. Vithal, B. Srinivasulu, K. Koteswara Rao, Ch. Mohan Rao, Mater. Lett. 45 (2000) 58–62.
[21] B.N. Figgis, Introduction to Ligand Fields, Wiley, New York, 1966.
[22] F. Mabbs, D.J. Machin, Magnetism and Transition Metal Complexes, Chapman & Hall, London, 1973.
[23] K. Nakamoto, Infrared and Raman Spectra of Inorganic and Coordination Compounds, third ed, Wiley-Interscience, New York, 1977, p. 142.
[24] F.A. Cotton, Chemical Applications of Group Theory, Wiley-Interscience, New York, 1971.
[25] D.M. Adams, D.C. Newton, Tables for Factor Group and Point Group Analysis, Beckmann, Croydon, 1970.
[26] C.E. Bamberger, G.M. Begun, O.B. Cavin, J. Solid. State Chem. 73 (1988) 317–324.
[27] C.E. Bamberger, G.M. Begun, J. Less-common Met. 134 (2) (1987) 201–206.
[28] A. El Jazouli, S. Krimi, B. Manoun, J.P. Chaminade, P. Gravereau, D. de Waal, Ann Chim. Sci. Mater. 23 (1998) 7–10.